




# A basis for customising perimetric locations within the macula in glaucoma

Muhammed S. Alluwimi , William H. Swanson, Victor E. Malinovsky and Brett J. King

School of Optometry, Indiana University, Bloomington, USA

**Citation information:** Alluwimi MS, Swanson WH, Malinovsky VE & King BJ. A basis for customising perimetric locations within the macula in glaucoma. *Ophthalmic Physiol Opt* 2018; 38: 164–173. <https://doi.org/10.1111/opo.12435>

**Keywords:** gaussian blob stimulus, glaucoma, macula, optical coherence tomography, perimetry, retinal nerve fibre layer bundles

*Correspondence:* Muhammed S Alluwimi  
E-mail address: malluwim@indiana.edu

Received: 15 June 2017; Accepted: 23 November 2017; Published Online: 8 January 2018

## Abstract

*Purpose:* It has been recognised that the 24-2 grid used for perimetry may poorly sample the macula, which has been recently identified as a critical region for diagnosing and managing patients with glaucoma. We compared data derived from patients and controls to investigate the efficacy of a basis for customising perimetric locations within the macula, guided by en face images of retinal nerve fibre layer (RNFL) bundles.

*Methods:* We used SD-OCT en face montages ([www.heidelbergengineering.com](http://www.heidelbergengineering.com)) of the RNFL in 10 patients with glaucoma (ages 56–80 years, median 67.5 years) and 30 age-similar controls (ages 47–77, median 58). These patients were selected because of either the absence of perimetric defect while glaucomatous damage to the RNFL bundles was observed, or because of perimetric defect that did not reflect the extent and locations of the glaucomatous damage that appeared in the RNFL images. We used a customised blob stimulus for perimetric testing (a Gaussian blob with 0.25° standard deviation) at 10-2 grid locations, to assess the correspondence between perimetric defects and damaged RNFL bundles observed on en face images and perimetric defects. Data from the age-similar controls were used to compute total deviation (TD) and pattern deviation (PD) values at each location; a perimetric defect for a location was defined as a TD or PD value of  $-0.5$  log unit or deeper. A McNemar's test was used to compare the proportions of locations with perimetric defects that fell outside the damaged RNFL bundles, with and without accounting for displacement of ganglion cell bodies.

*Results:* All patients but one had perimetric defects that were consistent with the patterns of damaged RNFL bundles observed on the en face images. We found six abnormal perimetric locations of 2040 tested in controls and 132 abnormal perimetric locations of 680 tested in patients. The proportions of abnormal locations that fell outside the damaged RNFL bundles, with and without accounting for displacement of the ganglion cell bodies were 0.08 and 0.07, respectively. The difference between the two proportions did not reach statistical significance ( $p = 0.5$  for a one-tailed test).

*Conclusions:* We demonstrated that it is effective to customise perimetric locations within the macula, guided by en face images of the RNFL bundles. The perimetric losses found with a 10-2 grid demonstrated similar patterns as the damaged RNFL bundles observed on the en face images.

Conventional automated perimetry has been widely used to diagnose and manage patients with glaucoma. It uses a standard grid that samples locations within the central  $\pm$

$30^\circ$  of the retina. This grid has locations that are separated by  $6^\circ$  in vertical and horizontal directions and there are only four points of this grid that sample the central  $\pm 8^\circ$  – which

is defined as the macular region in this study. This choice of testing grid was consistent with the assumption that the macula would be spared in most patients with glaucoma until advanced stages of the disease.

In the late twentieth century, several studies reported that perimetric defects in the macula could occur early in patients with glaucoma.<sup>1–4</sup> Meanwhile, the clinical impact of perimetric defects within the macula at early stages of glaucoma was not widely recognised because of the lack of corresponding structural data to support these results.

In the late 1990s, the importance of damage to the macula in early glaucoma had been demonstrated by measuring structural loss in patients with glaucoma.<sup>5</sup> With advances in imaging technology, several laboratories investigated the potential of detecting damage to the macula in patients with glaucoma.<sup>6–9</sup> Results from these studies confirmed that structural damage to the macula was frequently found in patients with glaucoma in all stages of the disease. This confirmation had led researchers to establish spatial comparisons between structural damage in the macula and corresponding perimetric defect using 10-2 locations in patients with glaucoma,<sup>10–15</sup> in which perimetric locations are 2° apart vertically and horizontally and cover the region of central ± 10°. The functional loss, in these studies, was confirmed in corresponding locations to the structural damage within the macula. These results emphasised the need for testing more perimetric locations at the macula than those used in the standard grid. However, it can be challenging for clinicians who make decisions on when the 24-2 or 10-2 test locations should be used.

To improve perimetric testing at the macula, Hood *et al.*<sup>16</sup> suggested that two perimetric locations could be added to the 24-2 grid to enhance perimetric sampling at the macula. A study by Chen *et al.*<sup>17</sup> found that these two perimetric locations were also the most frequently affected macular locations in their patients with glaucoma. This approach was based on probability maps created by measuring thicknesses of circumpapillary retinal nerve fibre layer (cpRNFL) and segmented RNFL at the macula so that the path of the glaucomatous damage to the RNFL could be observed.<sup>18</sup> However, adding two fixed locations may not be optimal because of variation in location and extent of glaucomatous damage to the RNFL: these two locations could fall outside the damaged region, resulting in poor perimetric sampling.<sup>19</sup> To overcome this limitation, another approach<sup>20</sup> suggested adding 16 perimetric locations to the central 24-2 grid in order to provide better perimetric sampling of the glaucomatous defect to the macula. This approach may improve the perimetric sampling of the macula, however, testing time will be increased by approximately one-third.

An alternative approach should be considered to provide better sampling of the perimetric defect within the

macula in patients with glaucoma. Recently, en face images of the RNFL bundles have been commercially available in which RNFL bundles can be visualised at different distances from the inner limiting membrane (ILM).<sup>21</sup> We aimed to assess the efficacy of customising perimetric locations within the macula based on use of OCT en face images to identify local regions of macular damage. Perimetric defects found at the 10-2 locations were compared to the abnormal regions seen in the en face images of the RNFL bundles.

## Methods

### Participants

We recruited 10 patients with primary open angle glaucoma and 30 age-similar controls from an ongoing glaucoma study in our lab. For patients, the age range was from 56 to 80 years with a median of 68 years while for the controls the age range was from 46 to 77 years with a median of 55 years. These patients were selected based on two criteria: (1) the absence of perimetric loss (using the 24-2 pattern with Goldmann size III) within the macula while glaucomatous damage to the macula was observed on the structural measurements; and (2) perimetric loss was present, but not as large as glaucomatous damage to the macula observed on the structural measurements, indicating that perimetric defect did not reflect the extent and locations of the glaucomatous damage. The perimetric losses were identified based on following criteria: total deviation (TD) and pattern deviation (PD) maps as derived from the Humphrey Field Analyzer printouts had at least one location with  $p < 0.5\%$  and at least two contiguous locations with  $p < 1\%$ .

For the 10 patients and the first 10 age-similar controls, the protocol called for one perimetry and imaging session because these participants had prior experience with our customised perimetry. The age range for the first 10 controls was from 55 to 77 years, with a median of 68. For the remaining age-similar controls, the testing protocol called for two visits in order to reduce the impact of learning effects because these participants were new to the customised perimetry testing station. The age range was from 46 to 76 years with a median of 54 years. We expect little effect of the age difference on our analysis because, as reported, the decrease in the visual sensitivity per decade is approximately 0.5 dB.<sup>22</sup>

The purpose of the study was explained to each participant before the testing sessions. Each participant gave signed, informed consent. This research was approved by the Indiana University Institutional Review Board. The protocol of this study adhered the tenets of Declaration of Helsinki.

### Inclusion criteria

Inclusion criteria were a comprehensive eye examination within the last 3 years; best-corrected visual acuity of 20/20 (0.0 logMAR or 6/6) or better, except for participants older than 70 years for whom 20/40 (0.30 logMAR or 6/12) was acceptable; and spherical equivalent from + 2.0 dioptres to -6.0 dioptres, with a cylinder < 3.0 dioptres. Additional inclusion criteria were the absence of systemic disease currently affecting visual function; medications that could significantly impair visual function; or history of intraocular surgery, except for glaucoma surgery and uncomplicated cataract surgery more than a year before enrolment. For all participants and at every visit, we evaluated their visual acuity and then measured contrast sensitivity using the Pelli-Robson chart. If there were changes in either of these two tests, the clinicians reviewed the participant's clinical chart to investigate the reason for the change.

### Exclusion criteria

For both patients and age-similar controls, we excluded participants who had ocular disease (other than glaucoma) known to affect visual function, including diabetic retinopathy, prior vein occlusion, macular degeneration, degenerative myopia, and the presence of significant ocular media opacity on an ophthalmic exam. An additional exclusion criterion for patients was intraocular pressure (IOP) > 30 mm Hg under current treatment. For controls, we excluded participants who had a primary relative with glaucoma, IOP > 21 mm Hg for the most recent clinic visit, abnormal disc appearance (definite signs consistent with glaucoma such as regional rim narrowing, notching or wedge-shaped RNFL defects), and abnormal fundus appearance.

### Equipment

#### *Spectralis OCT*

En face images of the RNFL were acquired using OCT (www.heidelbergengineering.com). We used vertical dense B-scans, 30 microns apart, composing four rectangles that covered much of the central  $\pm 30^\circ$ . The width and height of the first rectangle were  $25^\circ \times 20^\circ$ , and the temporal fixation target was used so that the operator placed the rectangle temporal to the fovea. The second and third scans were each designed to cover a retinal area of  $10^\circ \times 20^\circ$ . These scans were set to image superior and inferior macular regions by using fixation targets above and below the fovea. The fourth scan covered a  $15^\circ \times 30^\circ$  rectangle which was centred on the optic disc, using the nasal fixation target. Participants were dilated to allow rapid OCT imaging.

These images were acquired following a protocol designed for an ongoing study of structure-function relations in patients with glaucoma.

The volume scans were exported from the Spectralis OCT and read by a custom MATLAB (www.mathworks.com) program, which was developed by our lab. This custom program was used to montage volume scans for different regions of the retina into a single volume scan and provided en face images at different depths from the ILM. Reflectance was computed at given distances from the ILM by interpolating pixels above and below the region of interest.

We used en face images to identify glaucomatous damage to the RNFL bundles within the macula. However, it was challenging to identify damage to the RNFL bundles at a fixed distance from the ILM because of differences in the RNFL thickness between the temporal (thin RNFL) and the nasal (thick RNFL) portions of the macula. It has been reported that the RNFL thickness at the region temporal to the fovea is approximately 20 microns, while the nasal portion thickness is about 40 microns.<sup>23</sup> This means that if the distance from the ILM was increased more than 20 microns to better characterise glaucomatous damage at the nasal region of the macula, the RNFL bundles in the temporal region (thin portion) would not be visualised. Therefore, different distances from the ILM were used for different retinal regions in order to better visualise the damage to the RNFL bundles around the macula.

One of the authors was trained to determine the damage to the RNFL bundles on the en face images, this training included evaluation of over 100 cases of control and patient participants. In control participants, the RNFL bundles are densely packed at the macular region; therefore, the reflectance is uniformly distributed around the macula. Outside the macula, RNFL bundles appeared as striations taking an arcuate path to the optic disc. In patients, an arcuate defect appeared as a dark band indicating low reflectance of the RNFL bundles with glaucomatous damage.

To confirm the pattern of glaucomatous damage predicted based on the damage to the RNFL bundles as seen on the en face images, perimetric testing was employed at the macula using the 10-2 locations. We used a blob stimulus that is defined by a two-dimensional Gaussian with a standard deviation (SD) of  $0.25^\circ$  (Figure 1); this stimulus is similar in size to the Goldmann size III stimulus ( $0.43^\circ$  diameter). Such blob stimuli produce a soft transition at the edges of the stimulus unlike the hard edges of the Goldmann size III, and have been found to reduce test-retest variability.<sup>24</sup> We used a ZEST algorithm, as previously described,<sup>24,25</sup> to measure contrast sensitivity, in which stimulus locations were randomly presented.

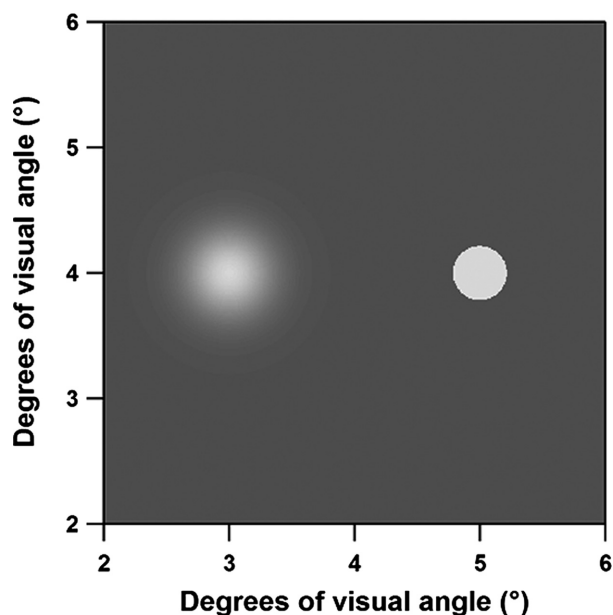


**Figure 1.** Blob stimulus (left) with  $0.25^\circ$  standard deviation (SD) of the Gaussian window with smooth edges as compared to the Goldmann size III ( $0.43^\circ$ ) on the right.

### Perimetry

We presented blob stimuli using a customised perimetry station that has been previously described.<sup>26</sup> In brief, we used a cathode-ray tube (CRT) system, controlled by a visual stimulus generator (ViSaGe); ([www.crsLtd.com](http://www.crsLtd.com)) with a screen resolution of  $800 \times 600$  pixels subtending  $51^\circ$  by  $42^\circ$  of visual angle. This system was operated by a custom MATLAB program to present the blob stimuli and to implement the strategies for perimetric testing. The background luminance was  $20 \text{ cd/m}^2$  and the maximum stimulus luminance was  $100 \text{ cd/m}^2$ . There was a motorised headrest to control head position. A camera was attached to the testing station to monitor fixation. A lens holder was centred in front of the screen at a distance of 33 cm; the participant's spherical equivalent with correction for this distance was used for the perimetric testing.

### Statistical analysis

In order to define abnormal sensitivities using blob stimuli in patients with glaucoma, total deviation (TD) and pattern deviation (PD) maps<sup>27</sup> were created for each participant. The TD for each location was computed as the difference from mean normal. The PD for each location was computed as TD with adjustment for the height of the hill of vision, which was calculated as the seventh highest value of TD for a participant subtracted from the average of the seventh highest TDs for the controls. For each location, abnormality was defined as any value equal or deeper than  $-0.5$

log unit in the TD and/or PD values. The value of  $-0.5$  log unit was selected based on very few abnormal locations found in the control group using this criterion. Also,  $-0.5$  log unit is clinically meaningful for the reduction of perimetric sensitivity.

For patients with glaucoma, the 10-2 locations were superimposed on the montaged en face images of the RNFL bundles to obtain a spatial comparison between the structural and functional measures. We aligned the visual field points with the en face images by identifying the foveal location based on foveal reflectance observed on the en face images and the location of the blind spot from previous perimetric exams, using standard 24-2 grid. This observation was performed with and without accounting for the displacement of the ganglion cell bodies.<sup>28</sup> We calculated the proportions of locations with perimetric defects that fell outside the visible damage to the RNFL bundles, with and without accounting for the displacement of the ganglion cell bodies. These two proportions were compared using a McNemar's test.

### Results

The TD and PD values of patients with glaucoma and age-similar controls are shown in *Figure 2*. Of 2040 perimetric locations in the age-similar controls, six locations in three participants were flagged as abnormal (0.3%). The standard deviation ranged across locations from 0.20 to 0.09 log unit for TD and from 0.17 to 0.07 log unit for PD. Of 680 perimetric locations tested in patients, perimetric abnormality was found at 132 locations (19%). Abnormal perimetric locations were found in nine of the 10 patients with glaucoma. The number of abnormal locations in patients ranged from 2 to 26, TD values ranged from  $+0.62$  to  $-1.45$  log unit and PD values ranged from  $+0.45$  to  $-1.50$  log unit. It can be observed from *Figure 2* (middle and third panel) that abnormal perimetric locations based on the results of the PD and TD were mostly in the superior visual field, locations numbered from 1 to 34. The average time of testing for controls was (minutes: seconds) 11:26 and for patients was 11:12.

The TD maps showed six abnormal locations found in three controls (*Figure 3*, left column), which were not contiguous. The PD maps showed one control with one abnormal location (*Figure 3*, right column, second plot). Perimetric defects, in most cases of patients with glaucoma, were consistent with our predictions based on observations from the en face images of the RNFL bundles (*Figure 4*). Data from one patient did not show abnormal locations in the TD map, but the PD map showed two abnormal locations. These two locations were consistent with structural damage seen on the en face images (*Figure 4*, second row). There was one patient whose data did not show abnormal



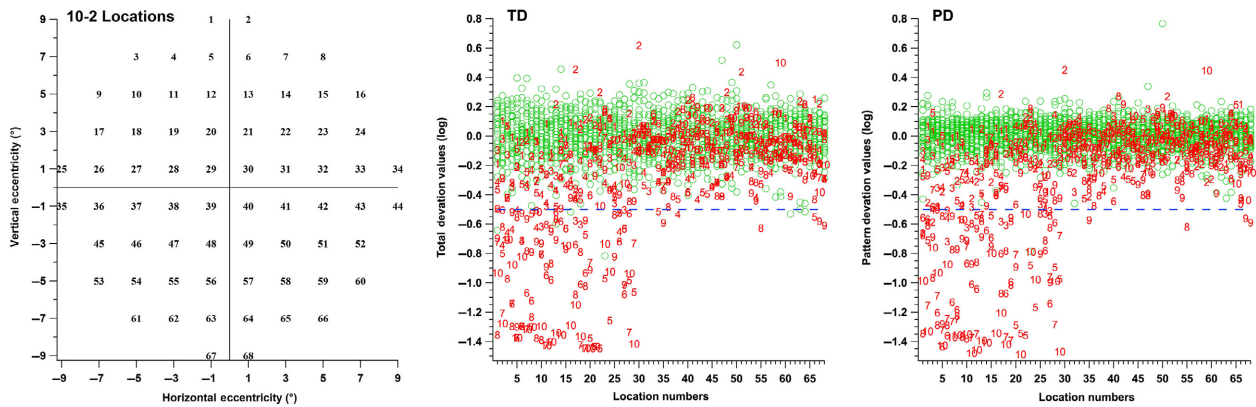


**Figure 2.** Distributions of the total deviation (TD) and pattern deviation (PD) values on the y-axis as a function of location number on the 10-2 grid (left panel). Green circles represent control data and the red numbers indicate patient data. It can be observed that most defects in the patient data were for locations in superior visual field, locations 1 to 34. The TD and PD values demonstrated similar results.

perimetric locations in TD and PD maps (*Figure 4*, top row) or damage to the RNFL bundles within the macula. Locations with glaucomatous damage as seen on the en face images and perimetric defects for each patient are summarised in *Figure 4*; images are ordered from lowest to the highest based on number of abnormal locations.

The proportions of abnormal perimetric locations that fell outside the damaged RNFL bundles, with and without accounting for the displacement of the ganglion cell bodies, were 0.08 and 0.07, respectively. The difference between these two proportions was 0.01 ( $p = 0.5$  for a one-tailed test).

## Discussion

In this study we presented preliminary data on the use of OCT en face images of the RNFL bundles to predict perimetric defects in the macula. The goal was to investigate the efficacy of a basis for customising perimetric locations within the macula. Patients in this study were selected based on either of two criteria. First, absence of perimetric defect within the macula using the 24-2 grid while there was structural damage within the macula. Second, perimetric defect was present but did not correspond to the structural damage within the macula. The evaluation of the structural damage was based on the observation on the en face images of the RNFL bundles with viewing glaucomatous damage at different distances for the ILM. In most cases, glaucomatous damage seen on the en face images was consistent with locations of perimetric defect within the macula. These findings were consistent with previous reports in which perimetric defects were found at corresponding locations of structural loss within the macula due to glaucoma.<sup>10-12,29</sup> This indicates that customising perimetric locations within the

macula will be effective in characterising glaucomatous damage.

Concordance between structural and functional damage was present in nine of 10 patients with glaucoma. The one remaining patient, who did not have damage to the RNFL within the macula, (*Figure 4*, first row) had a glaucomatous perimetric defect at the far periphery. Another patient had subtle glaucomatous damage (*Figure 4*, second row) in which the TD map did not show abnormal perimetric locations, but the PD map demonstrated two abnormal locations consistent with RNFL damage seen on the en face images. This may indicate that TD maps could underestimate perimetric loss if there is a high hill of vision in patients with subtle damage, and PD maps could be an alternative method to estimate abnormal perimetric locations with subtle damage. It should be noted that the technique presented in this study was applied on patients who had local and/or arcuate RNFL defects. It will be challenging to customise perimetric locations within the macula in cases of diffuse RNFL loss within the macula.

Between-subject variability in location of macular damage may limit the previously proposed approach.<sup>16,17</sup> These variations could be related to the biological differences between subjects such as the location of the optic nerve head<sup>30,31</sup> and foveal-disc angle.<sup>23</sup> The use of the high-resolution en face images could be used as an alternative approach to visualise the RNFL bundles at different depths from the ILM. One factor that may contribute to the between-subject variation is the displacement of ganglion cell bodies. In this study, a small difference was found in the proportion of the abnormal perimetric locations that fell outside the RNFL damage, with and without accounting for the displacement of ganglion cell bodies. This is an important finding because, with and without accounting for the displacement, we confirmed that there was a good

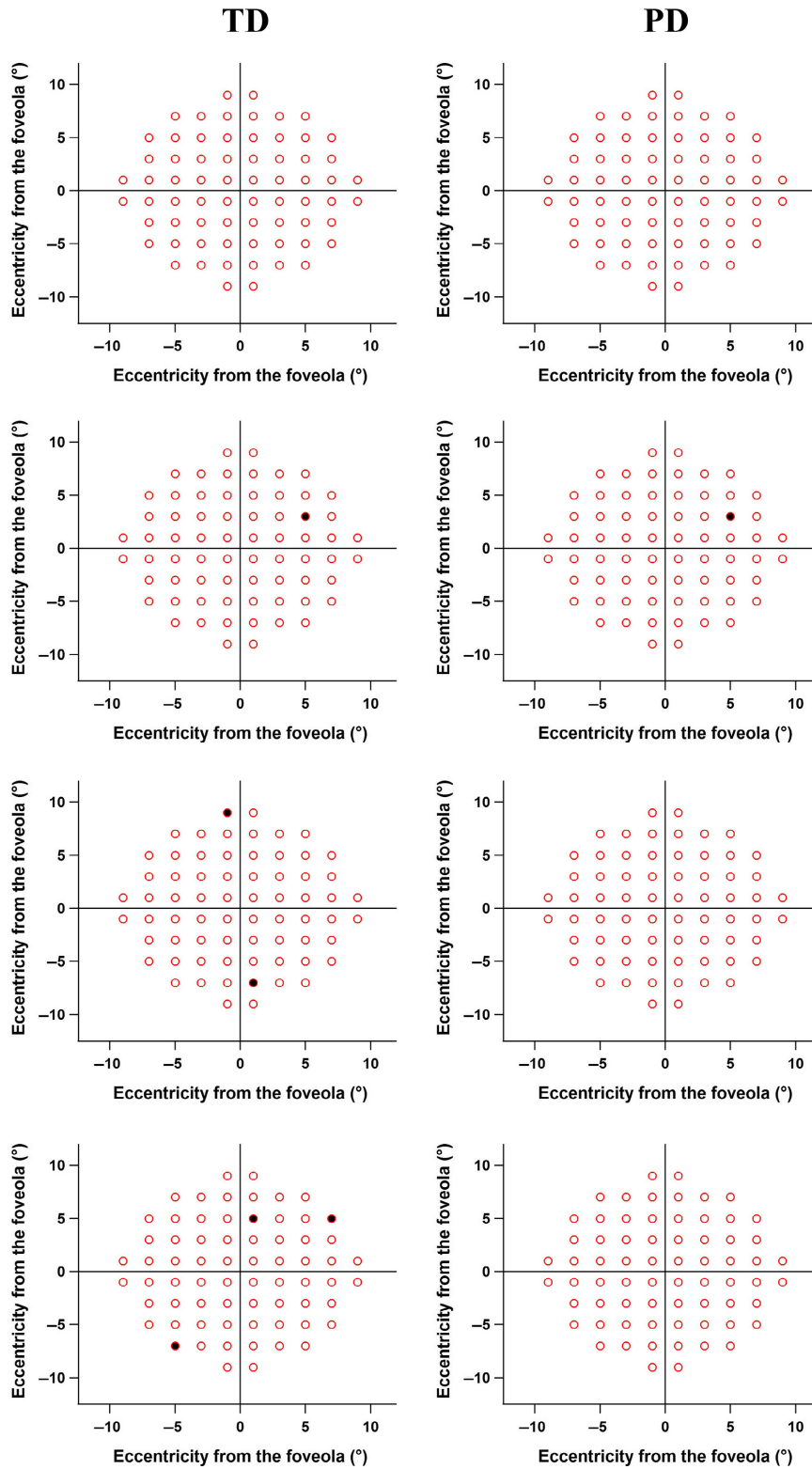


**Figure 3.** Total Deviation (TD) and Pattern Deviation (PD) maps from 30 control participants. The top row represents plots for 27 participants where no abnormal perimetric locations were found. The second row shows a control participant whose data showed one abnormal perimetric location in both TD and PD maps. The third and fourth rows demonstrated abnormal perimetric locations in TD maps but not in the PD maps.

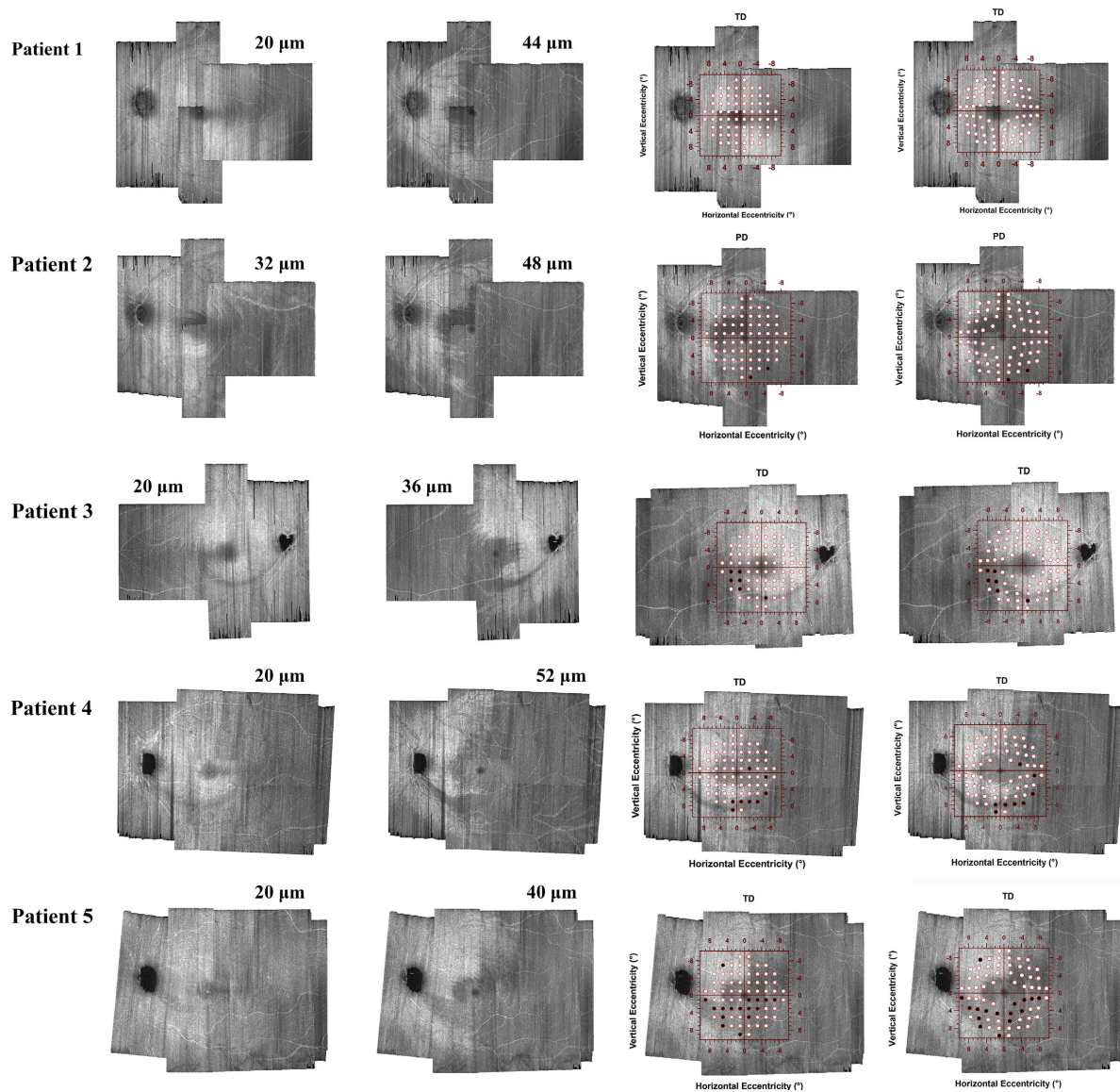


**Figure 4.** Results from individual patients with glaucoma. The two left columns demonstrate depths used with en face images to better characterise the glaucomatous damage. The first column indicates superficial depths (ranging from 16 to 20 microns from the ILM) while the second column indicates deeper depths (ranging from 32 to 52 microns). The third and fourth columns show the TD values of the 10-2 grid superimposed on the en face images with (fourth column) and without (third column) accounting for the displacement of ganglion cell bodies, black circles indicate abnormal perimetric locations. TD values were similar to PD, except for a patient in the second row in which PD was shown because the TD map did not show abnormal locations. The y-axis of the visual field map was flipped in order to correspond to retinal coordinates.

correspondence between the locations of the damaged RNFL bundles and abnormal perimetric locations.

The change of the depth from the ILM with the en face images can be beneficial because of the differences in the RNFL thickness nasal and temporal to the fovea. Using a single distance from the ILM to identify glaucomatous damage would show details of the damage to RNFL bundles temporal to the fovea while a deeper depth of the RNFL can be used in the region nasal to the fovea, because larger

distances from the ILM are required to characterise mild to moderate thinning of the RNFL. Therefore, at least two distances from the ILM through the RNFL were used to better characterise the width and locations of the glaucomatous damage on the en face images.

In order to identify glaucomatous damage to the RNFL bundles as it appeared in the en face images, one of the authors was trained to identify the patterns of glaucomatous damage by evaluating over 100 en face images of patients with



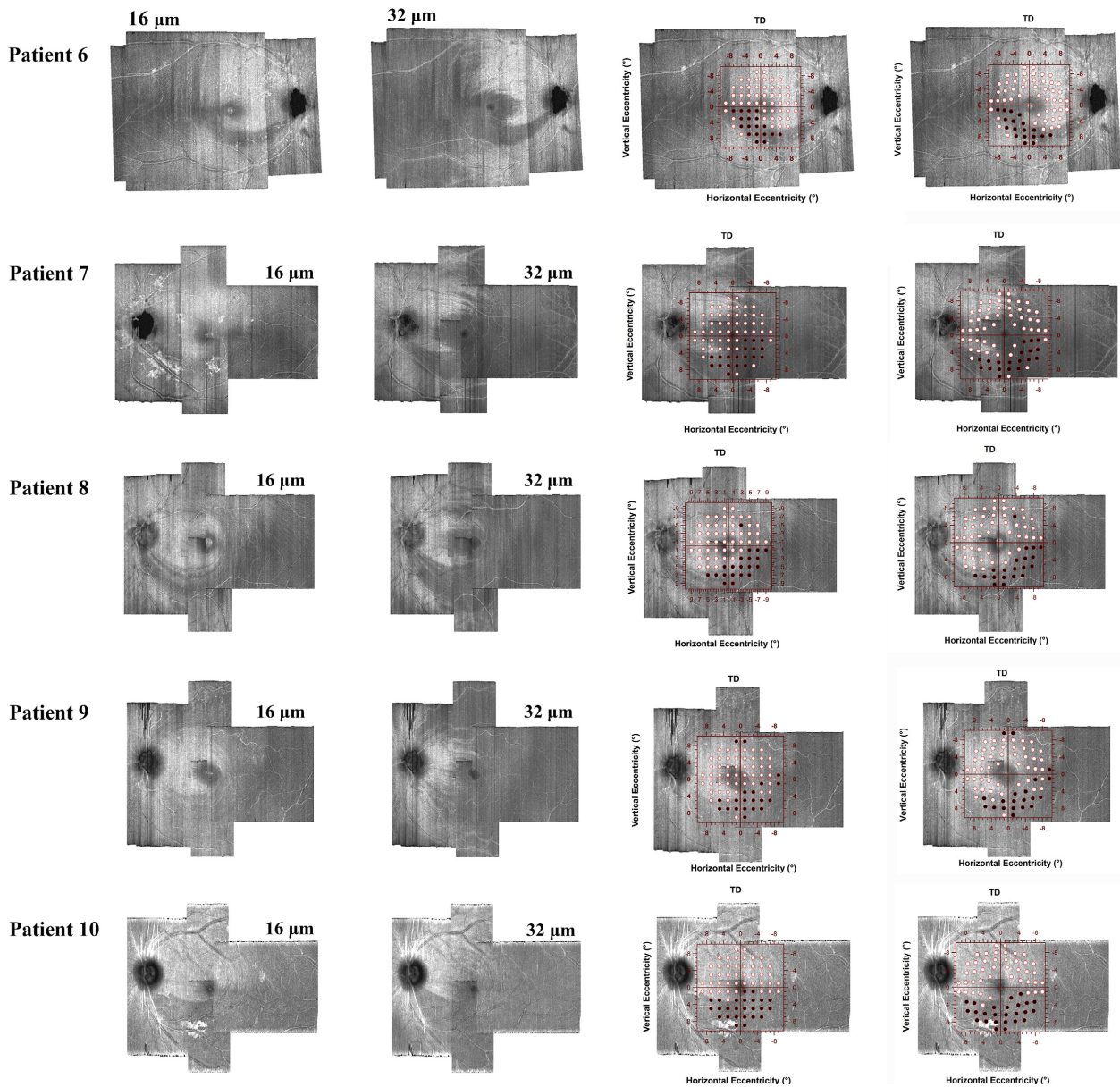


Figure 4. Continued

glaucoma and control participants. It will be worthwhile to investigate the potential of quantitative analysis of the en face images in patients with glaucoma. The quantification would lead to automatic identification of glaucomatous damage to the RNFL bundles, which could be confirmed with manual identification as we did in this study. Another important step could be using a perimetric method such as our approach in this study to assess the correspondence with the automatic quantification of the glaucomatous damage on the en face images. A later stage of the analysis could be to investigate possible methods to automatically quantify damage to the RNFL

bundles and present customised perimetric locations based on that structural quantification. This will help the investigation of potentially adding perimetric locations within the macula to the 24-2 grid in order to improve the perimetric sampling for the macula.

In conclusion, we presented preliminary data on the macula in patients with glaucoma in which locations of functional defects were consistent with structural loss. This indicates that the use of structural changes within the macula in patients with glaucoma may be effective to guide attempts to individualise perimetric locations within the macula.



## Acknowledgements

This work was supported by the US National Institutes of Health (grant R01EY024542).

## Disclosure

WHS is a consultant for Carl Zeiss Meditec and Heidelberg Engineering. MSA, VEM and BJK report no conflicts of interest and have no proprietary interest in any of the materials mentioned in this article.

## References

1. Ancil JL & Anderson DR. Early foveal involvement and generalized depression of the visual field in glaucoma. *Arch Ophthalmol* 1984; 102: 363–370.
2. Stamper RL. The effect of glaucoma on central visual function. *Trans Am Ophthalmol Soc* 1984; 82: 792–826.
3. King D, Drance SM, Douglas GR & Wijsman K. The detection of paracentral scotomas with varying grids in computed perimetry. *Arch Ophthalmol* 1986; 104: 524–525.
4. Lachenmayr BJ & Drance SM. Diffuse field loss and central visual function in glaucoma. *Ger J Ophthalmol* 1992; 1: 67–73.
5. Zeimer R, Asrani S, Zou S, Quigley H & Jampel H. Quantitative detection of glaucomatous damage at the posterior pole by retinal thickness mapping. A pilot study. *Ophthalmology* 1998; 105: 224–231.
6. Guedes V, Schuman JS, Hertzmark E *et al.* Optical coherence tomography measurement of macular and nerve fiber layer thickness in normal and glaucomatous human eyes. *Ophthalmology* 2003; 110: 177–189.
7. Lederer DE, Schuman JS, Hertzmark E *et al.* Analysis of macular volume in normal and glaucomatous eyes using optical coherence tomography. *Am J Ophthalmol* 2003; 135: 838–843.
8. Ishikawa H, Stein DM, Wollstein G, Beaton S, Fujimoto JG & Schuman JS. Macular segmentation with optical coherence tomography. *Invest Ophthalmol Vis Sci* 2005; 46: 2012–2017.
9. Garvin MK, Abramoff MD, Kardon R, Russell SR, Wu X & Sonka M. Intraretinal layer segmentation of macular optical coherence tomography images using optimal 3-D graph search. *IEEE Trans Med Imaging* 2008; 27: 1495–1505.
10. Kanadani FN, Hood DC, Grippio TM *et al.* Structural and functional assessment of the macular region in patients with glaucoma. *Br J Ophthalmol* 2006; 90: 1393–1397.
11. Wang M, Hood DC, Cho JS *et al.* Measurement of local retinal ganglion cell layer thickness in patients with glaucoma using frequency-domain optical coherence tomography. *Arch Ophthalmol* 2009; 127: 875–881.
12. Raza AS, Cho J, de Moraes CG *et al.* Retinal ganglion cell layer thickness and local visual field sensitivity in glaucoma. *Arch Ophthalmol* 2011; 129: 1529–1536.
13. Hori N, Komori S, Yamada H *et al.* Assessment of macular function of glaucomatous eyes by multifocal electroretinograms. *Doc Ophthalmol* 2012; 125: 235–247.
14. Takahashi M, Omodaka K, Maruyama K *et al.* Simulated visual fields produced from macular RNFLT data in patients with glaucoma. *Curr Eye Res* 2013; 38: 1133–1141.
15. Lee JW, Morales E, Sharifipour F *et al.* The relationship between central visual field sensitivity and macular ganglion cell/inner plexiform layer thickness in glaucoma. *Br J Ophthalmol* 2017; 101: 1052–1058.
16. Hood DC, Nguyen M, Ehrlich AC *et al.* A test of a model of glaucomatous damage of the macula with high-density perimetry: implications for the locations of visual field test points. *Transl Vis Sci Technol* 2014; 3: 5.
17. Chen S, McKendrick AM & Turpin A. Choosing two points to add to the 24-2 pattern to better describe macular visual field damage due to glaucoma. *Br J Ophthalmol* 2015; 99: 1236–1239.
18. Hood DC, Raza AS, de Moraes CG *et al.* Initial arcuate defects within the central 10 degrees in glaucoma. *Invest Ophthalmol Vis Sci* 2011; 52: 940–946.
19. Hood DC. Improving our understanding, and detection, of glaucomatous damage: an approach based upon optical coherence tomography (OCT). *Prog Retin Eye Res* 2017; 57: 46–75.
20. Ehrlich AC, Raza AS, Ritch R & Hood DC. Modifying the conventional visual field test pattern to improve the detection of early glaucomatous defects in the central 10 degrees. *Transl Vis Sci Technol* 2014; 3: 6.
21. Chauhan BC, Sharpe GP & Hutchison DM. Imaging of the temporal raphe with optical coherence tomography. *Ophthalmology* 2014; 121: 2287–2288.
22. Heijl A, Lindgren G & Olsson J. Normal variability of static perimetric threshold values across the central visual field. *Arch Ophthalmol* 1987; 105: 1544–1549.
23. Hood DC, Raza AS, de Moraes CG, Liebmann JM & Ritch R. Glaucomatous damage of the macula. *Prog Retin Eye Res* 2013; 32: 1–21.
24. Swanson WH, Horner DG, Dul MW & Malinovsky VE. Choice of stimulus range and size can reduce test-retest variability in glaucomatous visual field defects. *Transl Vis Sci Technol* 2014; 3: 6.
25. King-Smith PE, Grigsby SS, Vingrys AJ, Benes SC & Supowit A. Efficient and unbiased modifications of the QUEST threshold method: theory, simulations, experimental evaluation and practical implementation. *Vision Res* 1994; 34: 885–912.
26. Swanson WH, Malinovsky VE, Dul MW *et al.* Contrast sensitivity perimetry and clinical measures of glaucomatous damage. *Optom Vis Sci* 2014; 91: 1302–1311.
27. Heijl A, Lindgren A & Lindgren G. Test-retest variability in glaucomatous visual fields. *Am J Ophthalmol* 1989; 108: 130–135.
28. Drasdo N, Millican CL, Katholi CR & Curcio CA. The length of Henle fibers in the human retina and a model of

- ganglion receptive field density in the visual field. *Vision Res* 2007; 47: 2901–2911.
29. Schiefer U, Papageorgiou E, Sample PA *et al.* Spatial pattern of glaucomatous visual field loss obtained with regionally condensed stimulus arrangements. *Invest Ophthalmol Vis Sci* 2010; 51: 5685–5689.
  30. Denniss J, McKendrick AM & Turpin A. An anatomically customizable computational model relating the visual field to the optic nerve head in individual eyes. *Invest Ophthalmol Vis Sci* 2012; 53: 6981–6990.
  31. Lamparter J, Russell RA, Zhu H *et al.* The influence of inter-subject variability in ocular anatomical variables on the mapping of retinal locations to the retinal nerve fiber layer and optic nerve head. *Invest Ophthalmol Vis Sci* 2013; 54: 6074–6082.

## Supporting Information

Additional Supporting Information may be found in the online version of this article:

- Data S1.** 24-2 visual field printout for patient 1.
- Data S2.** 24-2 visual field printout for patient 2.
- Data S3.** 24-2 visual field printout for patient 3.
- Data S4.** 24-2 visual field printout for patient 4.
- Data S5.** 24-2 visual field printout for patient 5.
- Data S6.** 24-2 visual field printout for patient 6.
- Data S7.** 24-2 visual field printout for patient 7.
- Data S8.** 24-2 visual field printout for patient 8.
- Data S9.** 24-2 visual field printout for patient 9.
- Data S10.** 24-2 visual field printout for patient 10.